Helo, C., M.-A. Longpré, N. Shimizu, D. A. Clague, and J. Stix (2011), Explosive eruptions at mid-ocean ridges driven by CO_2-rich magmas, Nature Geosci, 4(4), 260-263, doi:10.1038/ngeo1104.
http://www.nature.com/ngeo/journal/v4/n4/full/ngeo1104.html

Explosive eruptions at mid-ocean ridges driven by CO_2-rich magmas

Christoph Helo*[1], Marc-Antoine Longpré[1], Nobumichi Shimizu[2], David A. Clague[3], John Stix[1]

[1]*Department of Earth & Planetary Sciences, McGill University, 3450 University Street, Montreal H3A 2A7, Canada*

[2]*Woods Hole Oceanographic Institution, 266 Woods Hole Road, Woods Hole, MA 02543, USA*

[3]*Monterey Bay Aquarium Research Institute, 7700 Sandholdt Road, Moss Landing, CA 95039, USA*

*corresponding author, email: christoph.helo@mail.mcgill.ca

The abstract

The abundance of volatile compounds, and particularly CO_2, in the upper oceanic mantle affects the style of volcanic eruptions. At mid-ocean ridges, eruptions are generally dominated by the gentle effusion of basaltic lavas with a low volatile content. But, explosive volcanism has been documented at some ocean spreading centres[1-3], indicative of abundant volatile compounds. Estimates of the initial CO_2 concentration of primary magmas can be used to constrain the CO_2 content of the upper oceanic mantle, but these estimates vary greatly[4,5]. Here we present ion microprobe measurements of the CO_2 content of basaltic melt trapped in plagioclase crystals. The crystals are derived from volcanic ash deposits erupted explosively at Axial Seamount, Juan de Fuca Ridge, in the northeast Pacific Ocean. We report unusually high CO_2 concentrations of up to 9,160 ppm, which indicate that the upper oceanic mantle is more enriched in carbon than previously thought. And we furthermore suggest that CO_2 fluxes along mid-ocean ridges[4,5] vary significantly. Our results demonstrate that elevated fluxes of CO_2 from the upper oceanic mantle can drive explosive eruptions at mid-ocean ridges.

Mid-ocean ridges (MOR) are the most active and voluminous volcanic systems on Earth, forming nearly 60 % of the Earth's crust. Owing to its large volume, MOR volcanism is a key contributor to the total CO_2 flux from the mantle to the Earth's surface. Recent work has documented the widespread existence of volcaniclastic ash deposits comprising basaltic glass fragments at MOR sites[1-3]. Although widely interpreted as primary products of submarine explosive eruptions[1,2,6], some researchers argue for lava-seawater interaction[7,8]. Due to its low solubility, CO_2 is the only magmatic volatile phase undergoing significant exsolution as basaltic magma ascends to the seafloor[9], hence the only volatile which can drive explosive eruptions at these

depths. Pyroclastic activity in MOR environments therefore is controlled by the primary CO_2 content of basaltic liquids, and consequently by the carbon budget of the mantle source. Initial CO_2 contents of variously enriched basalts from the Mid-Atlantic Ridge, including so-called "popping rock", are inferred to be between 660 and 57,600 ppm, based on their vesicularity and extent of carbon isotope fractionation[5,10]. However, such elevated CO_2 levels have never been measured directly. By contrast, dissolved CO_2 concentrations in vapour-undersaturated melt inclusions from an East Pacific Rise MOR basalt (MORB) suite, which are thought to represent the initial MORB volatile contents, show very low CO_2 contents of 44-244 ppm (ref. 4). This large discrepancy poses a significant problem to our understanding of CO_2 abundances in the MORB mantle and derived magmas.

We analysed the dissolved volatile concentration of 47 melt inclusions entrapped in plagioclase (An_{81-91}) prior to eruption as well as host glass shards sampled from five pyroclastic ash sequences on Axial Seamount (Supplementary Tables S1, S2), to assess the pre-eruptive volatile inventory of the local MORB. The Axial caldera system is part of the intermediate-rate spreading Juan de Fuca Ridge (JdFR) between 45° 50' N and 46° N. A present-day magma reservoir is present at 2.5-6 km beneath the volcanic edifice[11]. Widespread ash deposits up to 2 m thick on the volcano's flanks include angular glass fragments, thin platy glass shards interpreted as bubble walls and termed limu o Pele (Supplementary Fig. S1), and plagioclase phenocrysts. This volcanic ash is evidence for explosive activity accompanying effusive lava flows.

The melt inclusions are generally more primitive (7.85 to 10.85 wt % MgO) and more variable in their trace element composition than the host glass (Supplementary Fig. S2a, Supplementary Tables S1, S3). Incompatible trace element compositions

(Supplementary Fig. S2b) fall within the overall range of JdFR basalts[12] indicating some variations in the mantle source chemistry. The melt inclusions exhibit an extremely large range of CO_2 concentrations, from 262 ppm up to 9,159 ppm (Fig. 1), with ~30 % of the inclusions >1,000 ppm ("high-CO_2" inclusions). Corresponding saturation pressures range from ~ 60 MPa to 1.2 GPa (using ref. 13). These are the highest CO_2 concentrations ever measured in a MORB, and are consistent with previous predictions of initial, undegassed volatile contents of MORB liquids[5,10,14,15]. Variations of other volatile elements are much more restricted. H_2O concentrations are 0.12-0.38 wt %, S 825-1,379 ppm , Cl 14 – 144 ppm, and F 74-222 ppm. For comparison, melt inclusions from similar volcaniclastic deposits at the Gakkel Ridge record lower CO_2 concentrations between 170-1,600 ppm[16].

Decompression degassing of CO_2-rich, H_2O-poor magma results in exsolution of CO_2 with restricted H_2O partitioning into the vapour phase[9]. Within CO_2-H_2O space, the melt inclusions define a vertical trend (Fig. 1), indicating volatile saturation and decompression degassing of CO_2-rich vapour from mantle to crustal depths (40 km to 2 km, calculated from the range of CO_2-H_2O saturation pressures, and a crustal density of 2,360 kg m^{-3}, ref. 17). H_2O variability exceeds that expected from purely degassing trends. The excellent positive correlation between H_2O and F in the melt inclusions (Fig. 2a) indicates their similar geochemical behaviour and a constant H_2O/F of the local mantle source of 14.3±0.1. Hence, the H_2O variability reflects some heterogeneity of the mantle source.

The ratio also allows us to assess post-eruptive alteration in MORBs, as hydration by seawater will cause the ratio to vary as a function of H_2O. Moreover, Cl/H_2O in the melt inclusions varies only as a function of Cl (Fig. 2b). Cl is accordingly assimilated

within the magma reservoir, while H_2O is not. Figure 2 reveals that the host glasses show both hydration and Cl assimilation. Hence Cl/H_2O and H_2O/F combined can be used to assess both the degree of pre-eruptive Cl assimilation and post-eruptive seawater-alteration in MORBs.

During melting, volatiles such as CO_2 behave highly incompatibly and partition strongly into the melt phase, similar to elements such as Nb (ref. 4). The melt inclusion with the highest CO_2 concentration (9,159 ppm) is volatile-oversaturated at any pressure below 1.2 GPa (calculated using ref. 13). Subsequent evolution of primitive CO_2-rich melts, as they ascend from the upper mantle to the shallow magma reservoir, can be evaluated in terms of three conceptual CO_2 degassing scenarios. First, degassing during ascent in the mantle without crystallisation would not entrap high-CO_2 melts and can be ruled out. Second, the melt inclusions show no correlation between the degree of fractionation in terms of their Ca-number or Mg-number and CO_2 content (Supplementary Fig. S3), which would be expected for continuous coeval degassing and crystallisation of plagioclase or olivine during magma ascent in the mantle. We therefore propose a third scenario where melt entrapment occurs over shallower mantle to crustal depths, in agreement with the calcic composition of the plagioclase crystals (Supplementary Table S4),which is commonly associated with crystallisation at lower pressures[18,19]. Following the model in ref. 19, melt is entrapped as magma rises through a calcic plagioclase-rich zone within the magma plumbing system. This implies that significant volatile exsolution is delayed during the ascent of melt batches from the deeper mantle, introducing strong degrees of supersaturation. The CO_2 bubble nucleation rate depends on the extent of supersaturation, with the degree of supersaturation necessary for bubble nucleation increasing at lower pressures as magma

rises[20]. As the supersaturated magma arrives and stagnates at constant pressures within the magma reservoir system at ~6 km depth, it will then experience strong CO_2 exsolution. In a similar fashion, strong degrees of supersaturation are achieved during the ascent of magma from the reservoir to the seafloor, as clearly demonstrated by our CO_2 data from the host glasses (Fig. 1b) and previous studies[5,9].

Our documentation of high CO_2 levels in primitive MORB liquid has far-reaching implications. The data provide insights into the physical evolution of the magma as it passes through the mantle into the shallow reservoir and is then erupted. At saturation pressures of ~60 MPa corresponding to a crustal depth of 2 km (using ref. 17), at least 8800 ppm CO_2 have been exsolved from a magma initially containing 9,160 ppm CO_2, translating to a vesicularity of ~10 % of free vapour. At the ocean floor this increases to ~32-34 % vesicularity. Under these conditions, expanding bubbles rising within the conduit can coalesce and drive strombolian explosions. For conditions similar to Axial Seamount, ref. 21 models a maximum magma rise velocity of 0.5-2.0 m s^{-1} and a vent width of 0.3-0.6 m for bubble coalescence to be achieved. Alternatively, bubbles could accumulate against the reservoir roof of the magma reservoir as a foam layer[22]. When a critical thickness of foam is reached, an eruption is triggered by foam collapse at the top of the reservoir, and gas slugs rise through the conduit causing bubble bursts. We compute a minimum gas flux of ~10^{-1} kg s^{-1} for the foam to reach the critical height using a gas fraction in the foam of 0.76 and a bubble radius of 0.3 mm (see supplementary information for calculations). The two models are not mutually exclusive. If an eruption is triggered before the critical foam thickness is reached, the accumulated foam will enhance bubble coalescence within the conduit, resulting in strombolian activity according to the first model. In both scenarios, erupting gas pockets

138 are separated by low vesicularity melt, as syn-eruptive degassing adds less than 4 % to
139 the total vesicularity. Our key conclusion is that the very high CO_2 in the mantle and
140 derived magmas gives rise to large amounts of CO_2-rich gas bubbles at shallow crustal
141 levels, which in turn drive explosive submarine eruptions.

142 Adopting a CO_2/Nb of ~4,000 from the least degassed melt inclusion, a similar
143 geochemical behaviour of both elements during melting[4] and a Nb abundance of the
144 mean upper depleted mantle of 0.3 ppm (ref. 23), we calculate a minimum CO_2 content
145 of 1200 ppm for the mantle source beneath Axial Seamount (corresponding to 330 ppm
146 of elemental carbon). For the 100 km spreading segment supplied by Axial Seamount
147 we find a carbon mantle flux of 23×10^8 mol yr^{-1}, using a magma production rate
148 constrained by the thickness of the local crust[24] of 6-8 km and a spreading rate of 6 mm
149 yr^{-1}. Likewise, using a global oceanic crust production rate of 20±3 km^3 yr^{-1} (ref. 25)
150 and a mean N-MORB Nb content of 3.5±1.9 ppm (ref. 23), we estimate a carbon mantle
151 flux of $19\pm10 \times 10^{12}$ mol yr^{-1} at mid-ocean ridges. This flux agrees with previous high
152 estimates of 15×10^{12} mol yr^{-1} (ref. 10) and exceeds the lower range of estimates by
153 nearly an order of magnitude[5,16].

154 CO_2 and Nb data from a number of studies from the last ten years[4,5,26,27] suggest
155 variable CO_2/Nb in parts of the upper mantle rather than a constant value (Fig. 3). If
156 both elements behave identically during mantle processes[4], their ratio should remain
157 constant and independent from the elemental concentrations. However, CO_2 and Nb
158 contents from various locations reveal a strong tendency towards lower CO_2/Nb as CO_2
159 decreases (Fig. 3). Hence, the CO_2 variability is much greater than Nb, suggesting either
160 degassing of volatile-saturated magma, or a heterogeneous carbon distribution in the
161 mantle that is decoupled from non-volatile incompatible elements such as Nb. While the

CO_2-H_2O data from Axial suggest strong decompression degassing, results for Siqueiros[4] and the North Atlantic ridge[5] (14 °N and 34 °N) are thought to represent undegassed CO_2 contents. Only data for the North Atlantic ridge at 14 °N show constant CO_2/Nb. All other localities appear to be affected by CO_2 degassing, heterogeneous mantle carbon distributions, or both.

Our data provide evidence of extremely high dissolved CO_2 concentrations in primitive, volatile saturated MORB magmas at depths of 35-40 km. The high CO_2 content of mantle-derived MORB magmas at Axial Seamount establishes a direct link with explosive eruptions and widespread pyroclastic deposits at MOR spreading centres. We propose that CO_2 is decoupled from other incompatible elements in parts of the upper mantle, and CO_2 fluxes can vary significantly along mid-ocean ridges.

Methods

Volatile (H_2O, CO_2, S, F, and Cl) analysis was carried out at Woods Hole Oceanographic Institution (WHOI) utilising high mass resolution secondary ion mass spectrometry (CAMECA IMS 1280). Selection of melt inclusions was done carefully through observations under transmitted and reflected light avoiding cracks or shrinkage bubbles within inclusions. Plagioclase grains with exposed inclusions were mounted into indium metal, and a 0.3 µm alumina oxide suspension was used for final polish. Prior to gold-coating, the mounts were dried in a vacuum oven at 110° C and 10^{-3} torr for ~12 h and were stored under vacuum at 10^{-7} torr for ~24 h. They were further allowed to outgas in the machine airlock at 3×10^{-9} torr. Sample chamber pressures during analysis were $<5 \times 10^{-9}$ torr. The principal analytical procedure followed the method as described in ref. 28. The detected secondary ions (^{12}C, $^{16}O^{1}H$, ^{19}F, ^{30}Si, ^{32}S,

and ^{35}Cl) were produced by a primary $^{133}Cs^{+}$ beam of 1.2-1.5 nA current and 15 µm diameter. An electron beam was employed to compensate for positive charging of the sample surface. The primary beam was rastered over a 30×30 µm area, and a mechanical aperture was placed at the secondary ion image plane, such that the central 15×15um area was analyzed after 3 min of pre-sputtering. Counting times of 10 s were used for ^{12}C and $^{16}O^{1}H$, and 5 s for ^{19}F, ^{30}Si (reference mass), ^{32}S and ^{35}Cl. Data were acquired over 10 blocks. Magnet positions were calibrated for every spot and mass resolving power was set to > 6,700 to resolve interferences of ^{17}O from $^{16}O^{1}H$ and $^{29}Si^{1}H$ from ^{30}Si. Nine standard glasses, of basaltic and basaltic andesite compositions, were used to establish calibration curves for $^{12}C/^{30}Si$, $^{16}O^{1}H/^{30}Si$, $^{19}F/^{30}Si$, $^{32}S/^{30}Si$, and $^{35}Cl/^{30}Si$ versus the respective volatile component. CO_2 content of all standard glasses was determined by Fourier transform infrared (FTIR) spectroscopy after the method of ref. 29. The standard error on the slope of the calibration curves is 2.4 % for CO_2 and 4.8 % or better for H_2O, F, S, and Cl. The 1σ stability of the $^{12}C/^{30}Si$ signal during analyses was better than 10 %, except for sample PlgM1_3-1 (12.2 %) and PlgM2_7-1 (14.1 %). The 1σ reproducibility of the in-run standard glass P1326-2, a JdFR basalt, was 5.3 % or better for CO_2, F, S and Cl, and 7.8 % for H_2O. Details on standards and quality of analyses are given in Supplementary Tables S5 and S6, and Supplementary Figs S4–S6. Special care was taken to verify high CO_2 contents in melt inclusions: first, nine high-CO_2 melt inclusions were re-analyzed after removing gold with 0.3 µm Al_2O_3 suspension. Potential surface contamination was reduced by sputter-cleaning melt inclusions with a stronger ion beam (5 nA) for 5 minutes, instead of a regular cleaning procedure with a 1.5-nA beam. Duplicate analyses confirmed the high CO_2 concentrations initially obtained. The data reported here are the duplicate values.

Second, secondary ion images of ^{12}C were observed for each melt inclusion, and a homogeneous distribution of ^{12}C was confirmed for melt inclusions. No enrichment of CO_2 in cracks or edges of melt inclusions was observed. Third, ^{12}C intensity during analysis did not display any sign of surface contamination (Supplementary Fig. S5). Fourth, the CO_2 concentration in host plagioclase adjacent to melt inclusions was much less than 30 ppm. This is considered to represent the CO_2 background.

Subsequent to the volatile analysis, trace element compositions were determined for the melt inclusions using a CAMECA IMS 3f secondary ion mass spectrometer at WHOI[30]. Calibration was carried out using the KL2-G glass standard. Trace element concentrations of the in-run standard P1326-2 were reproducible at a $1\sigma < 8$ %, except for Ba (11 %) (Supplementary Table S6). Major element compositions for the melt inclusions and the host glasses were analysed by electron microprobe (JEOL 8900) at McGill University, using a beam current of 1.5 nA, 15 kV, and defocused beam of 5 µm diameter for the melt inclusions and 10 µm for the host glasses.

References

1. Clague, D. A., Davis, A. S. & Dixon, J. E. in *Explosive Subaqueous Volcanism* (eds White, J. D. L., Smellie, J. L. & Clague, D. A.) (American Geophysical Union, Washington, DC, 2003).

2. Clague, D. A., Paduan, J. B. & Davis, A. S. Widespread strombolian eruptions of mid-ocean ridge basalt. *J. Volcanol. Geotherm. Res.* **180**, 171-188 (2009).

3. Sohn, R. A. *et al.* Explosive volcanism on the ultraslow-spreading Gakkel ridge, Arctic Ocean. *Nature* **453**, 1236-1238 (2008).

4. Saal, A. E., Hauri, E. H., Langmuir, C. H. & Perfit, M. R. Vapour undersaturation in primitive mid-ocean-ridge basalt and the volatile content of Earth's upper mantle. *Nature* **419**, 451-455 (2002).

5. Cartigny, P., Pineau, F., Aubaud, C. & Javoy, M. Towards a consistent mantle carbon flux estimate: Insights from volatile systematics (H_2O/Ce, δD, CO_2/Nb) in the North Atlantic mantle (14 degrees N and 34 degrees N). *Earth Planet. Sci. Lett.* **265**, 672-685 (2008).

6. Davis, A. S. & Clague, D. A. in *Explosive Subaqueous Volcanism* (eds White, J. D. L., Smellie, J. L. & Clague, D. A.) (American Geophysical Union, Washington, DC, 2003).

7. Clague, D. A., Davis, A. S., Bischoff, J. L., Dixon, J. E. & Geyer, R. Lava bubble-wall fragments formed by submarine hydrovolcanic: explosions on Lo'ihi Seamount and Kilauea Volcano. *Bull. Volcanol.* **61**, 437-449 (2000).

8. Maicher, D. & White, J. D. L. The formation of deep-sea Limu o Pele. *Bull. Volcanol.* **63**, 482-496 (2001).

9. Dixon, J. E. & Stolper, E. M. An experimental study of water and carbon dioxide solubilities in mid-ocean ridge basaltic liquids. 2. Applications to degassing. *J. Petrol.* **36**, 1633-1646 (1995).

10. Javoy, M. & Pineau, F. The volatiles record of a "popping rock" from the Mid-Atlantic Ridge at 14 ° N: chemical and isotopic composition of gas trapped in the vesicles. *Earth Planet. Sci. Lett.* **107**, 598-611 (1991).

11. West, M., Menke, W., Tolstoy, M., Webb, S. & Sohn, R. Magma storage beneath Axial volcano on the Juan de Fuca mid-ocean ridge. *Nature* **413**, 833-836 (2001).

12. PetDB. Petrological Database of the Ocean Floor, http://www.petdb.org.

13. Newman, S. & Lowenstern, J. B. VOLATILECALC: a silicate melt-H_2O-CO_2 solution model written in Visual Basic for excel. *Comput. Geosci.* **28**, 597-604 (2002).

14. Gerlach, T. M. Comment on "Mid-ocean ridge popping rocks: implications for degassing at ridge crests" by P. Sarda and D. Graham. *Earth Planet. Sci. Lett.* **105**, 566-567 (1991).

15. Hekinian, R. *et al.* Deep sea explosive activity on the Mid-Atlantic Ridge near 34 degrees 50 ' N: Magma composition, vesicularity and volatile content. *J. Volcanol. Geotherm. Res.* **98**, 49-77 (2000).

16. Shaw, A. M., Behn, M. D., Humphris, S. E., Sohn, R. A. & Gregg, P. M. Deep pooling of low degree melts and volatile fluxes at the 85 degrees E segment of the Gakkel Ridge: Evidence from olivine-hosted melt inclusions and glasses. *Earth Planet. Sci. Lett.* **289**, 311-322 (2010).

17. Gilbert, L. A., McDuff, R. E. & Johnson, H. P. Porosity of the upper edifice of Axial Seamount. *Geology* **35**, 49-52 (2007).

18. Grove, L. T., Kinzler, R. J. & Bryan, W. B. in *Mantle Flow and Melt Generation at Mid-Ocean Ridges* (eds Morgan, J. P., Blackman, D. K. & Sinton, J. M.) (American Geophysical Union, Washington, DC, 1992).

19. Nielsen, R. L. *et al.* Melt inclusions in high-An plagioclase from the Gorda Ridge: an example of the local diversity of MORB parent magmas *Contrib. Mineral. Petrol.* **122**, 34-50 (1995).

20. Bottinga, Y. & Javoy, M. Midocean ridge basalt degassing - bubble nucleation. *J. Geophys. Res.* **95**, 5125-5131 (1990).

21. Head, J. W. & Wilson, L. Deep submarine pyroclastic eruptions: theory and predicted landforms and deposits. *J. Volcanol. Geotherm. Res.* **121**, 155-193 (2003).

22. Jaupart, C. & Vergniolle, S. The generation and collapse of foam layer at the roof of a basaltic magma chamber. *J. Fluid. Mech.* **203**, 347-380 (1989).

23. Hofmann, A. W. Chemical differentiation of the earth - the relationship between mantle, continental crust, and oceanic crust. *Earth Planet. Sci. Lett.* **90**, 297-314 (1988).

24. West, M., Menke, W. & Tolstoy, M. Focused magma supply at the intersection of the Cobb hotspot and the Juan de Fuca ridge. *Geophys. Res. Lett.* **30,** 1724, 4pp., doi:10.1029/2003GL017104 (2003).

25. Cogné, J. P. & Humler, E. Trends and rhythms in global seafloor generation rate. *Geochem. Geophys. Geosyst.* **7**, 17 (2006).

26. Shimizu, K. *et al.* CO_2-rich komatiitic melt inclusions in Cr-spinels within beach sand from Gorgona Island, Colombia. *Earth Planet. Sci. Lett.* **288**, 33-43 (2009).

27. Dixon, J. E. & Clague, D. A. Volatiles in basaltic glasses from Loihi seamount, Hawaii: Evidence for a relatively dry plume component. *J. Petrol.* **42**, 627-654 (2001).

28. Hauri, E. *et al.* SIMS analysis of volatiles in silicate glasses 1. Calibration, matrix effects and comparisons with FTIR. *Chem. Geol.* **183**, 99-114 (2002).

29. Fine, G. & Stolper, E. Dissolved carbon dioxide in basaltic glasses: concentrations and speciation. *Earth Planet. Sci. Lett*. **76**, 263-278 (1986).

30. Shimizu, N. & Hart, S. R. Applications of the ion-micro-probe to geochemistry and cosmochemistry. *Annu. Rev. Earth Planet. Sci.* **10**, 483-526 (1982).

Correspondence and requests for materials should be addressed to C.H.

Acknowledgments

The authors thank the Captain and crew of the R/V Western Flyer and the pilots of the ROV Tiburon for their support and expertise during the 2006 MBARI Vance Expedition. The expedition and DAC were supported through a grant to MBARI from the David and Lucile Packard Foundation. C.H. was supported

by R.H. Tomlinson, GEOTOP and J.W. McConnell Memorial Fellowships at McGill University. J.S. was supported by grants from the Natural Sciences and Engineering Research Council of Canada. We thank Dr. Bruce Watson from the Rensselaer Polytechnic Institute for synthesising the high-CO_2 glass standard NS-1, and Dr. Charles Mandeville from the American Museum of Natural History for the FTIR determination of CO_2 content of this standard.

Author contributions

C.H. performed volatile analysis and major element analysis of the melt inclusions and host glasses, and analysed the data. M.-A.L performed the trace element analysis of the melt inclusions, N.S. supervised the volatile and trace element analysis, D.A.C was responsible for the organisation of the cruise and sample collection, and J.S. supervised the work. The manuscript was written primarily by C.H., with contributions from M.-A.L., N.S., D.A.C., and J.S.

Additional information

The authors declare no competing financial interests. **Supplementary information** accompanies this paper on **www.nature.com/naturegeoscience**.

Figure 1 Dissolved CO_2 and H_2O contents in melt inclusions and host glasses, measured by SIMS. Isobars calculated using ref. 13. 1σ error bars are shown for representative values. **a**, Melt inclusions exhibit an extremely wide range in CO_2 contents. The vertical trend indicates decompression degassing from a volatile-saturated melt. **b**, Zoom of the region below 1,000 ppm CO_2. The host glasses are volatile-oversaturated for an eruption pressure of 14 MPa (grey isobar). Host glasses are equilibrated at crustal depths between 0.3 and 2 km. The continuity in CO_2 concentrations from melt inclusions to host glasses indicates limited syn-eruptive degassing.

Figure 2 H_2O, F, and Cl contents of the melt inclusions and host glasses. **a**, The excellent correlation between H_2O and F in the melt inclusions indicates similar geochemical behaviour and suggests H_2O/F in the mantle of 14.3±0.2 (2σ). The host glasses display increasing H_2O at roughly constant F, indicating hydration and alteration of the erupted basalt. **b**, Cl/H_2O in the melt inclusions is controlled solely by the amount of Cl assimilated within the magma reservoir. By contrast post-eruptive alteration of the host glasses increases both Cl and H_2O, causing Cl/H_2O to remain roughly constant. 1σ error bars are shown.

Figure 3 Bilogarithmic plot of CO_2/Nb versus CO_2. The wide range of observed CO_2/Nb is striking, generally decreasing with lower CO_2. This trend can be explained by either degassing of CO_2 from volatile-saturated magmas, or in cases where degassing can be ruled out, by CO_2 distribution in the mantle which is decoupled from Nb. Decoupling of these two elements would result in a range of initial CO_2/Nb. *Axial*: degassed, measured dissolved volatile content in melt inclusions; *Siqueiros* [4]: undegassed, measured dissolved volatile content in melt inclusions; *North Atlantic ridge* [5] *14°N* and *34°N* and *Loihi* [27]: reconstructed undegassed volatile contents.

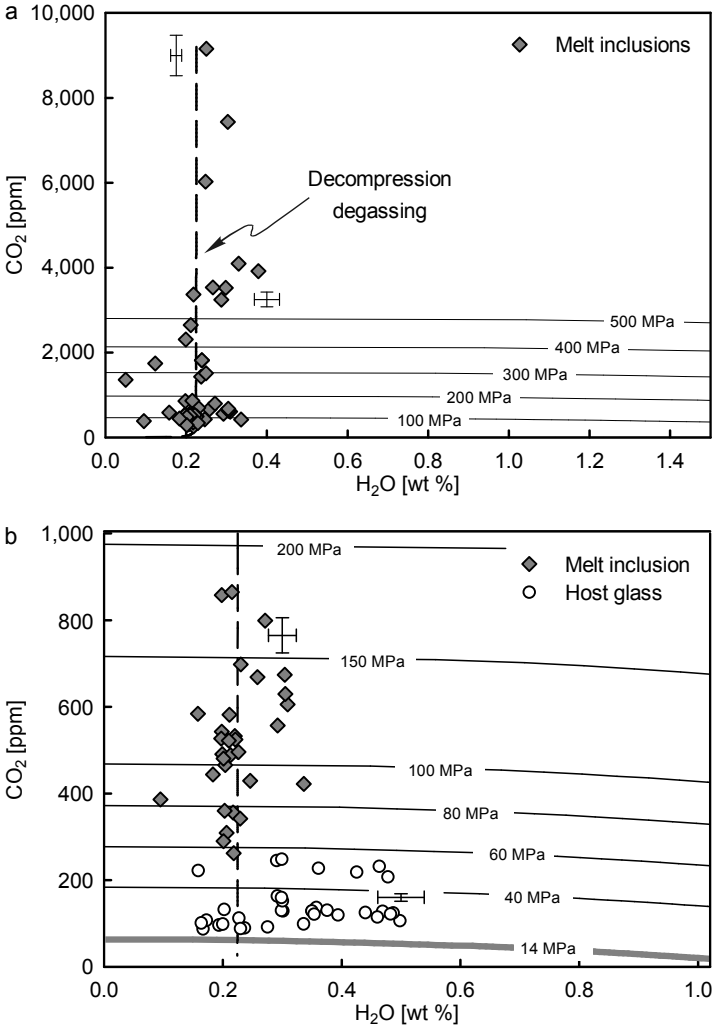
a
Melt inclusions
Decompression degassing
500 MPa
400 MPa
300 MPa
200 MPa
100 MPa
CO2 [ppm]
H2O [wt %]
b
Melt inclusion
Host glass
200 MPa
150 MPa
100 MPa
80 MPa
60 MPa
40 MPa
14 MPa
CO2 [ppm]
H2O [wt %]

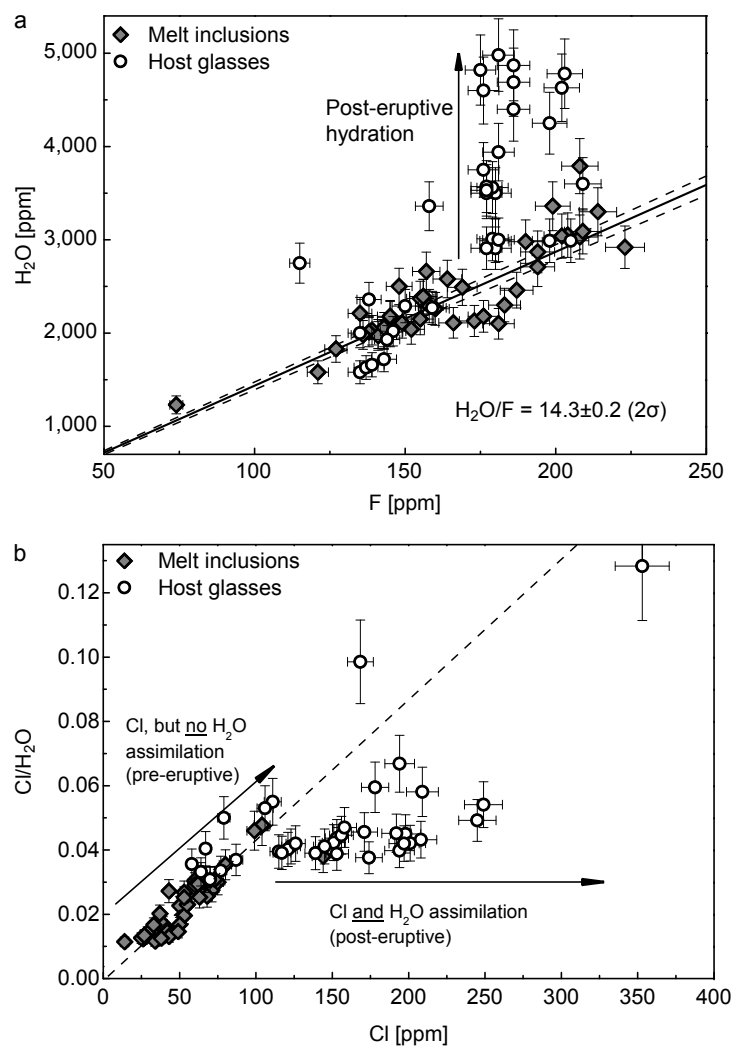
a
Melt inclusions
Host glasses
Post-eruptive hydration
H2O/F = 14.3±0.2 (2σ)
H2O [ppm]
F [ppm]
b
Melt inclusions
Host glasses
Cl, but no H2O assimilation (pre-eruptive)
Cl and H2O assimilation (post-eruptive)
Cl/H2O
Cl [ppm]

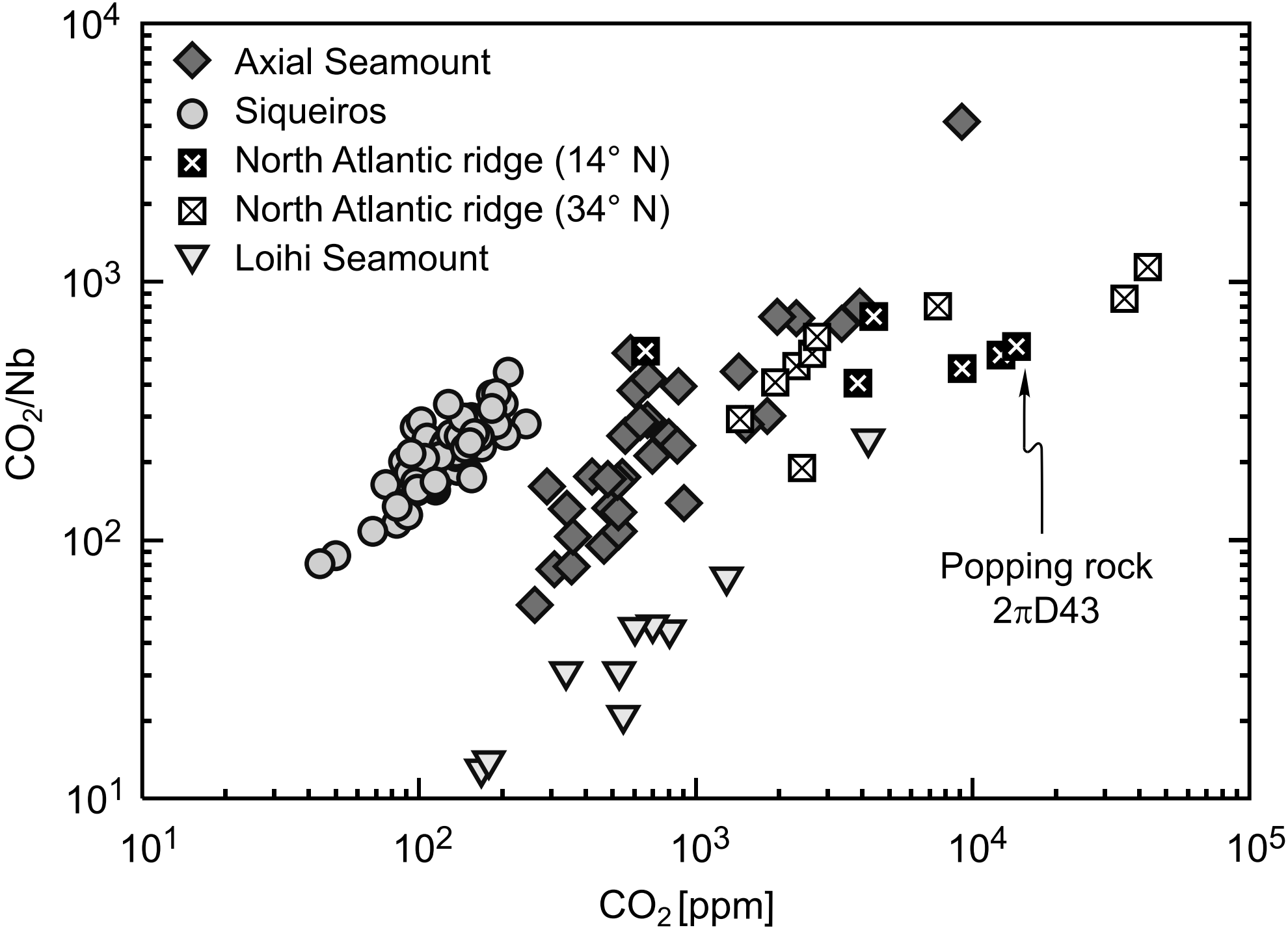
Axial Seamount
Siqueiros
North Atlantic ridge (14° N)
North Atlantic ridge (34° N)
Loihi Seamount
Popping rock
2πD43
CO_2/Nb
CO_2 [ppm]
10^1
10^2
10^3
10^4
10^5